JACS
JOURNAL OF THE AMERICAN CHEMICAL SOCIETY

ARTICLE

pubs.acs.org/JACS

Correlated Electron Dynamics: How Aromaticity Can Be Controlled

Inga S. Ulusoy* and Mathias Nest

Technische Universität München, Theoretische Chemie, Lichtenbergstrasse 4, 85747 Garching, Germany

Supporting Information

ABSTRACT: In this Article, we show that the aromaticity of a molecule can be turned off by controlling the electron dynamics. We present a controlled switching from the aromatic ground state of benzene to two different nonaromatic states, using a laser pulse. The propagation of the molecular wave function is carried out with the time-dependent configuration interaction method. The laser pulse for switching between the ground and excited states is optimized using optimal control theory. Bond orders and Mulliken charges serve as an aromaticity criterion. The nonaromatic target states exhibit localized bonds and partial charges on the carbon atoms; these localized electrons circulate on an attosecond time scale in the ring system.

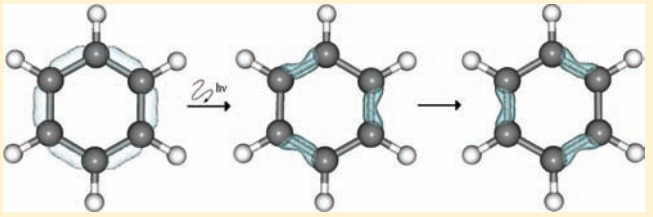

INTRODUCTION

With the control of molecular properties, molecular building blocks can be functionalized and fabricated into molecular devices and switches.[1] Using quantum control calculations, molecules can selectively be manipulated. For example, very large ring currents can be induced in aromatic compounds,[2,3] or selected rotational and vibrational excitations of the molecule can be targeted to trigger reactions.[4,5] Generally, the chemical properties of a molecule are governed by the valence electrons. Thus, by controlling the electron dynamics, we can control molecular properties,[6,7] such as the degree of aromaticity of a molecule. Characteristics which are connected to aromaticity are, for example, a high stability (reduced reactivity), a high molecular symmetry, and that large paramagnetic ring currents can be induced which e.g. lead to a downfield shift in ^{1}H NMR. The complement of aromatic systems are antiaromatic systems, which are kinetically unstable (and thus highly reactive), avoid regular, symmetric structures and exhibit diamagnetic ring currents when a magnetic field is applied.

Generally, aromaticity is connected to the cyclic delocalization of π-electrons. This delocalization of the π-electrons is in fact enforced upon the system by the σ-electrons, which favor a highly symmetric structure with equal bond lengths.[8−12] The excited states of aromatic systems are generally less aromatic (since an electron is shifted from a bonding to an antibonding orbital), and often even antiaromatic.[13−15] Some interest has already been drawn to the first excited triplet states of cyclic hydrocarbons, where the $4n + 2$ π-electron rule for aromaticity and $4n$ π-electron rule for antiaromaticity is reversed (Baird's rules).[13] Aromaticity switches however have not yet received much attention. Nevertheless, a Hückel/Möbius aromaticity switch has been designed recently.[16]

In this paper, we present a controlled switching of benzene from the aromatic ground state to a nonaromatic state using a laser pulse. The pulse is determined by quantum optimal control theory. By now, many methods are available to simulate the correlated dynamics of electrons. This can either be done using a density-based method such as time-dependent density functional theory (TDDFT)[17,18] or a wave function based method. However, controlled dynamics are almost exclusively carried out using wave function based theories. Here, different methods have been developed, such as the time-dependent Hartree−Fock method (TD-HF)[19] and the multiconfiguration time-dependent Hartree−Fock method (MCTDHF).[20−23] While the former is too approximate for our purpose, the latter is difficult to use in combination with control algorithms.[24] Other methods which have been presented previously allow calculations of ionic states and dynamics beyond the Born−Oppenheimer approximation.[25,26] The method we use is the time-dependent configuration interaction method (TD-CI),[27,22] in combination with optimal control theory (OCT)[28] to optimize the laser pulse which is used for the switching between the states.

Many molecular properties are connected to the degree of aromaticity and can serve as aromaticity identifiers: The chemical behavior (favoring electrophilic substitution over addition), geometric criteria such as bond length equalization, the resonance energy (enhanced stability), the NICS (nucleus-independent chemical shift),[29,30] or for example, the ring current strength and direction induced by a magnetic field.[31,32] Many measures for the degree of aromaticity have been discussed,[30,33,34] but there is often no simple relation between them. This makes it very difficult to define aromaticity in the case of nonstandard situations, like (superpositions of) excited states, or nonequilibrium geometries. Since, in this work, we are dealing with electron dynamics which happen on a different time-scale than the nuclear motion, we need an aromaticity criterion which is independent of the nuclear positions. Mainly, we will use Mayer's bond orders[35] to identify the degree of aromaticity. The overlap

Received: July 4, 2011
Published: November 02, 2011

of the atomic orbitals (AOs), which are centered on different atoms, reflects chemical interactions between these atoms, and the bond orders thus measure the extent to which electrons are shared between pairs of atoms. In the aromatic ground state, six of the valence electrons of the carbon atoms are evenly shared in the π-bonds of the ring system. Thus, the bond orders of all bonds ideally have an equal value of 1.5. In a nonaromatic state such as a single Kekulé structure, these six π-electrons are localized and form double bonds between every second carbon atom, so that alternating bond orders of ideally 2.0 and 1.0 are obtained. Thus, bond orders can indicate nonaromatic states, as a state with localized electrons is no longer aromatic. We also calculate Mulliken charges[36] in order to identify partial charges on carbon atoms.

Other electron sharing indices have been used previously in correlated calculations,[37] yielding good results. However, we aim at a straightforward description of the bonding which can be interpreted directly. Additionally, good results and agreement with other indices was already obtained for bond orders.[38,39]

We first summarize the theoretical methods used in this work, and then present the results and conclusions. In the Results section, we use atomic units where $\hbar = 1$.

THEORY

TD-CISD. The simulations of the electron dynamics and time-dependent properties are carried out using the time-dependent CI method.[27,22] Starting from the RHF ground state, the CI space is constructed by adding singly and doubly excited determinants to the wave function. Benzene has 42 electrons, of which 24 inner-valence electrons are kept frozen in the CI calculation. The active space for the remaining 18 valence electrons contains all virtual orbitals for single excitations, and nine virtual orbitals for double excitations. Thus, we adapt the naming convention for CASSCF calculations and denote this ansatz CISD(18,18) for 18 electrons in the active space containing 18 spin−orbitals for double excitations. The CI matrix is diagonalized, and the CI ground state is the starting point for the time-dependent calculation. The time-dependent wave function $\Psi(\mathbf{r},t)$ is expressed in the eigenstate basis:

$$\Psi(\mathbf{r},t) = \sum_i C_i(t)|\Psi_{\mathrm{CI},i}(\mathbf{r})\rangle \tag{1}$$

Here, $\mathbf{r}$ contains the space and spin coordinates of all electrons. The Hamiltonian consists of the molecular Hamiltonian $\hat{H}_0$ and a time-dependent electric field $\vec{\varepsilon}(t)$,

$$\hat{H} = \hat{H}_0 - \vec{\mu}\vec{\varepsilon}(t) \tag{2}$$

with dipole moment $\vec{\mu}$. The time-dependent Schrödinger equation is solved using the split-operator technique.[40,41] Here, the propagator is split into different factors which are each represented in their eigenstate basis, in which the factors are diagonal: The molecular Hamiltonian is expressed in energy eigenstates and the electric field using the position basis. The basis transformation between the two representations is carried out using the transformation matrix $\mathbf{U}$. The CI coefficients at times $t + \Delta t$, $C_i(t + \Delta t)$, can then be expressed as

$$C_i(t + \Delta t) = \mathrm{e}^{-iE_i\Delta t/\hbar}\,\mathbf{U}^{\ddagger}\,\mathrm{e}^{-i\vec{\mu}\vec{\varepsilon}(t)\Delta t/\hbar}\,\mathbf{U}C_i(t) \tag{3}$$

When no electric field is present, only the phase factors change. All calculations are carried out using the equilibrium geometry of benzene in the RHF ground state (CC-bond length: 2.64 a_0, CH-bond length: 2.08 a_0; see Supporting Information) and using a 6-31G* Gaussian basis set.[42,43] The molecule is oriented in the xy-plane.

Optimal Control Theory. We construct a laser pulse which allows switching between the ground state and selected target states of benzene. The laser pulse is optimized using global optimal control theory (OCT).[28] OCT is an iterative method, in which the electric field is optimized in many steps of forward and backward propagation. In the forward propagation, the population of the electronic states is calculated for an electric field $\vec{\varepsilon}_n(t)$. In the subsequent backward propagation, this electric field is optimized, yielding a new electric field $\vec{\varepsilon}_{n+1}(t)$. These OCT cycles are repeated until convergence of the populations and the electric field is obtained. The first OCT cycle starts with a forward propagation using a trial pulse $\vec{\varepsilon}_0(t)$. At the final time T, the final state of the propagation $\Psi_f(T)$ is projected onto the target state Ψ_{target}, using a projection operator $\hat{O}$, and yields the starting point $\chi(T)$ for the backward propagation:

$$|\chi(T)\rangle = \hat{O}|\Psi_f(T)\rangle = |\Psi_{\mathrm{target}}\rangle\langle\Psi_{\mathrm{target}}|\Psi_f(T)\rangle \tag{4}$$

During the backward propagation, the laser field for times t, $\vec{\varepsilon}_1(t)$, is obtained by

$$\vec{\varepsilon}_1(t) = -\frac{1}{\alpha_0}\mathrm{Im}\langle\chi(t)|\vec{\mu}|\Psi(t)\rangle \tag{5}$$

α_0 is a positive parameter weighting the influence of the laser field. The state $\chi(t)$ is backward propagated by applying the complex conjugate of the propagation operator, eq 3, using the optimized laser field $\vec{\varepsilon}_1(t)$ in the exponent. The electric field is optimal when the functional J is maximized:

$$J = \langle\Psi_f(T)|\hat{O}|\Psi_f(T)\rangle - \frac{\alpha_0}{\hbar}\int_0^T[\vec{\varepsilon}_{\mathrm{opt}}(t)]^2\mathrm{d}t \tag{6}$$

J thus yields a convergence criterion of the algorithm. Only the 20 lowest singlet eigenstates of benzene were included in the OCT calculation.

Bond Orders and Charges. Once a switching between the ground and target states of benzene is achieved, we analyze these target states with respect to their aromaticity. For this analysis, we use Mulliken charges[36] and bond orders,[35] which are straightforward to calculate and can directly be interpreted. The Mulliken charges and bond orders are calculated from the time-dependent charge density bond order matrix $\mathbf{P}(t)$ (CDBO):

$$P_{\mu\nu}(t) = \langle\mu|Tr_{2\ldots n_{\mathrm{el}}}\{|\Psi(t)\rangle\langle\Psi(t)|\}|\nu\rangle \tag{7}$$

The CDBO matrix is expressed in the AO basis with nonorthogonal basis functions μ and ν. The overlap matrix $\mathbf{S}$ of the AOs contains the elements

$$S_{\mu\nu} = \langle\phi_\mu|\phi_\nu\rangle \tag{8}$$

The product of CDBO and overlap matrix, $\mathbf{PS}$, yields the density matrix from which the Mulliken charges and bond orders are calculated. The gross atom population $\mathrm{GAP_A}$ for atom A is defined as

$$\mathrm{GAP_A} = \sum_{\mu\in\mathrm{A}}\sum_{\nu}(\mathbf{PS})_{\mu\nu} \tag{9}$$

for AOs μ centered on A. The Mulliken charge Q_A is then calculated as

$$Q_\mathrm{A} = Z_\mathrm{A} - \mathrm{GAP_A} \tag{10}$$

with Z_A being the atomic number of atom A. The bond order B_{AB} of two neighboring atoms A and B is calculated as

$$B_{\mathrm{AB}} = \sum_{\mu\in\mathrm{A}}\sum_{\nu\in\mathrm{B}}(\mathbf{PS})_{\mu\nu}(\mathbf{PS})_{\nu\mu} \tag{11}$$

with AOs μ centered on A and ν centered on B. There have been discussions whether bond orders calculated from correlated wave functions should be defined using the second-order density matrix,[44,45] but we follow Mayer's suggestion and use the same definition as for single-determinantal wave functions.[35,45]

Table 1. Bond Orders, B_{AB}, and Mulliken Charges, Q_A, of the Ground and First Two Excited Singlet States of Benzene, and Superpositions of Singlet States

state	symmetry (point group)	B_{12}	B_{23}	B_{34}	B_{45}	B_{56}	B_{61}
S_0	$^1A_{1g}$ (D_{6h})	1.41	1.41	1.41	1.41	1.41	1.41
S_1	$^1B_{2u}$ (D_{6h})	1.21	1.21	1.21	1.21	1.21	1.21
S_2	$^1B_{1u}$(D_{6h})	1.24	1.24	1.24	1.24	1.24	1.24
$S_0 + S_1$ (i)	$^1A_{1g}$ (D_{3d})	1.04	1.75	1.04	1.75	1.04	1.75
$S_0 + S_2$ (ii)	$^1A_1'$ (D_{3h})	1.32	1.32	1.32	1.32	1.32	1.32
state	symmetry (point group)	Q_1	Q_2	Q_3	Q_4	Q_5	Q_6
S_0	$^1A_{1g}$ (D_{6h})	−0.19	−0.19	−0.19	−0.19	−0.19	−0.19
S_1	$^1B_{2u}$ (D_{6h})	−0.21	−0.21	−0.21	−0.21	−0.21	−0.21
S_2	$^1B_{1u}$ (D_{6h})	−0.21	−0.21	−0.21	−0.21	−0.21	−0.21
$S_0 + S_1$ (i)	$^1A_{1g}$ (D_{3d})	−0.20	−0.20	−0.20	−0.20	−0.20	−0.20
$S_0 + S_2$ (ii)	$^1A_1'$ (D_{3h})	0.05	−0.45	0.05	−0.45	0.05	−0.45

RESULTS AND DISCUSSION

We first identify interesting target states of benzene by calculating the bond orders and Mulliken charges of the low-lying excited states and superpositions thereof. Then, these target states are prepared starting from the electronic ground state, using a laser pulse. Finally, the target states are propagated in time, and we calculate time-dependent bond orders and Mulliken charges.

The bond orders and Mulliken charges of the ground and first two excited singlet states of benzene are shown in Table 1. The bond orders of the ground state of benzene ($^1A_{1g}$) are 1.41 for all CC bonds. Here, twelve electrons are involved in the σ-bonding between the carbon atoms, and almost five electrons are shared between pairs of atoms: Summing the bond orders of the six bonds and subtracting six single bonds leaves 4.92 π-electrons. The remaining charge to complete the six π-electrons bonded in the ring system is involved in multicenter bonding and thus not obtained by a summation over pairs of atoms.

The bond orders of the first two excited singlet states, S_1 ($^1B_{2u}$) and S_2 ($^1B_{1u}$) are smaller than in the ground state S_0, which is expected since one electron is shifted from a bonding to an antibonding orbital ($\pi^* \leftarrow \pi$ transition). However, electronic charge is still delocalized in the ring system. Previous studies have shown that the first excited singlet state of benzene is antiaromatic.[15] In antiaromatic compounds, the tendency of the π-electrons to form localized bonds overrules the preference of the σ-electrons for bond length equalization, due to symmetry reasons of the molecular orbitals (MOs).[8,11,12] Therefore, antiaromatic compounds avoid planar, regular structures (e.g., cyclobutadiene is rectangular[46]). Coming back to Table 1, it is apparent that the antiaromaticity of state S_1 is not obvious from the bond orders and Mulliken charges, since the electrons are still delocalized. We are thus not able to clearly distinguish aromatic and antiaromatic states by comparing bond orders and charges. However, we can turn this argument around and use bond orders and charges to identify states in which the electrons become localized, thus identifying nonaromatic states. We expect that the pure states of benzene can only be aromatic or antiaromatic, due to symmetry reasons. To find low-lying nonaromatic states, we calculate bond orders and Mulliken charges of the superpositions of S_0 and S_1 (each 50%, state (i)), as well as S_0 and S_2 (each 50%, state (ii)). These superpositions are built initially as the in-phase combinations of the respective states, where in the propagation the phases oscillate (see eq 3). State (i) shows an alternating bond pattern of single and almost double bonds, while the Mulliken charges remain constant, resembling the Kekulé structure. This state can also be viewed in terms of valence-bond theory: The aromatic ground state of benzene is the positive combination of the two Kekulé structures,[47,48] where the first excited state of benzene is the negative combination of these two structures. Thus, a 1:1 superposition of the ground and first excited state of benzene results in a single Kekulé structure, since in a sum of these two states, one of the Kekulé structures cancels.

Table 2. Energy Differences ΔE_{fi} (in E_h) and Transition Dipole Moments μ_{fi} (in ea_0) of Final and Initial State

$\|i\rangle$	$\|f\rangle$	$\mu_{fi,x}/ea_0$	$\mu_{fi,y}/ea_0$	$\Delta E_{fi}/E_h$
0	1	0.000	0.000	0.2138
0	2	0.000	0.000	0.2932
0	3	−1.775	0.000	0.3452
0	4	0.000	1.775	0.3452
0	5	0.000	0.000	0.3485
0	6	0.000	0.000	0.3485
1	3	0.000	0.000	0.1314
1	4	0.000	0.000	0.1314
1	5	−0.172	0.000	0.1347
1	6	0.000	0.172	0.1347
2	3	0.000	0.000	0.0520
2	4	0.000	0.000	0.0520
2	5	0.000	0.752	0.0553
2	6	0.752	0.000	0.0553
3	5	−0.349	0.000	0.0033
3	6	0.000	−0.349	0.0033
4	5	0.000	−0.349	0.0033
4	6	0.349	0.000	0.0033

State (ii) has slightly lower bond orders than the aromatic ground state. However, from the Mulliken charges it becomes apparent that electronic charge is accumulated at every second carbon atom. This results in alternating positive and negative partial charges and thus a more or less triply ionic structure. The second excited singlet state of benzene consists of several singly ionic structures,[48] therefore a superposition of ground and second excited state has substantial ionic character.

In the superposition states (i) and (ii), the symmetry of the benzene molecule is reduced from the D_{6h} point group to the D_{3d} (state (i)) and D_{3h} (state (ii)) point groups. The symmetries of the target states are given in Table 1.

States (i) and (ii) are nonaromatic states, since part of the electronic charge is localized. By exciting the benzene molecule from the ground state in one of these target states, the aromaticity of the molecule can be switched off.

Preparation of the Target States. After having identified nonaromatic target states, these states are populated starting from the electronic ground state using a laser pulse. First, a trial laser pulse is used as a starting point for the OCT calculation, and then iteratively optimized. The transition dipole moments and energy differences of the most important states are shown in Table 2.

The preparation of state (i) cannot be realized using a direct route, since an electronic transition between states S_0 and S_1 is forbidden by symmetry. We choose an alternative path via intermediate states. The envelope of the trial laser pulse is a $\sin^2$-function, where the intensity is calculated using a $\pi/2$-pulse formula for only 50% population transfer from state S_0 to S_3

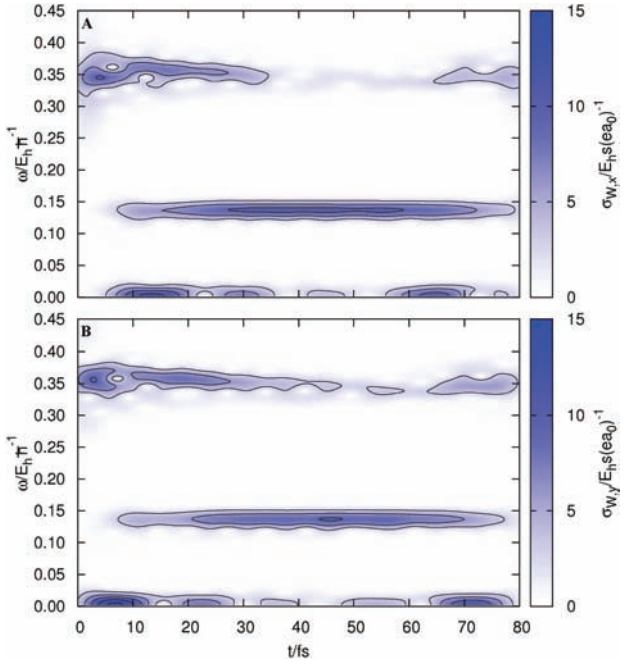

Figure 1. Time-dependent spectrum of the electric field for switching to target state (i), using a Gaussian sliding window. **A** *x*-component; **B** *y*-component of the electric field vector.

(see Supporting Information). In the following steps, 100% population from S_3 is shifted first to S_5 and then to S_1. The sequence followed during the trial pulse is

$$S_0 \rightarrow S_0 + S_3 \rightarrow S_0 + S_5 \rightarrow S_0 + S_1$$

The trial pulse is polarized in *x*-direction and 200 fs long. The trial laser pulse is then optimized using OCT until convergence of the electric field and the state populations is obtained ($\Delta J < 10^{-4}$). During the optimization, the electric field is allowed to change in *x*- and *y*-polarization direction, resulting in an elliptically polarized pulse.[49,50] Using a step function, that is, by setting the penalty for the laser field $\alpha_0 = 10^9\ (ea_0)^2 E_h^{-1}$ for the first and last 10 fs, the laser pulse is shortened successively to a duration of 80 fs. For shorter laser pulses, the final state contained less than 45% of S_1 and more than 55% of S_0, which we set as the tolerance limit for a deviation from a 1:1 superposition of S_0 and S_1. The parameter for the optimized electric field is $\alpha_0 = 2\ (ea_0)^2 E_h^{-1}$.

To analyze the frequency composition of the optimized laser pulse, the electric field was multiplied with a sliding Gaussian window function, and then Fourier-transformed. Here, 500 Gaussian functions $\exp(-(t - t_c)^2/2\sigma^2)$ were used, with the distance from one center t_c to the other 0.16 fs and σ =2.5 fs^{-1}. We obtain frequency maps for both *x*- and *y*-components of the electric field vector (Figure 1). At the start of the pulse, peaks are obtained at $\omega \approx 0.35\ E_h\hbar^{-1}$, which corresponds to the transitions $S_0 \rightarrow S_3$ (for the *x*-polarization direction) and $S_0 \rightarrow S_4$ (for the *y*-polarization direction). At $t \approx 2-5$ fs, frequencies of $\omega \approx 0.003\ E_h\hbar^{-1}$ are obtained, corresponding to a population transfer $S_3 \rightarrow S_5/S_6$ and $S_4 \rightarrow S_5/S_6$. At $t \approx 16$ fs, frequency components of about $0.134\ E_h\hbar^{-1}$ are obtained, corresponding to the transitions $S_5 \rightarrow S_1$ (*x*-polarization) and $S_6 \rightarrow S_1$ (*y*-polarization).

The populations of the respective states during the optimized laser pulse are shown in Figure 2. In the beginning of the propagation, the ground state S_0 is completely depopulated

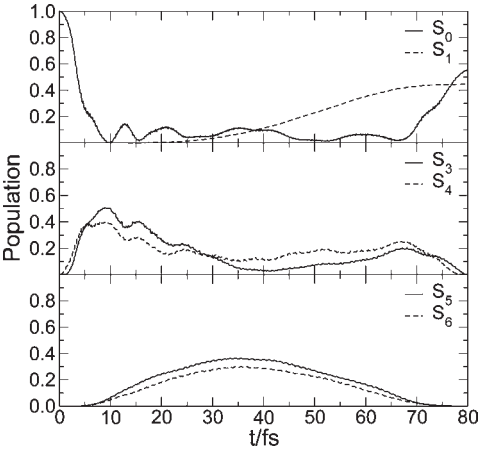

Figure 2. Populations of the electronic states involved in the population transfer from the ground state S_0 to the superposition of S_0 and S_1 (state (i)).

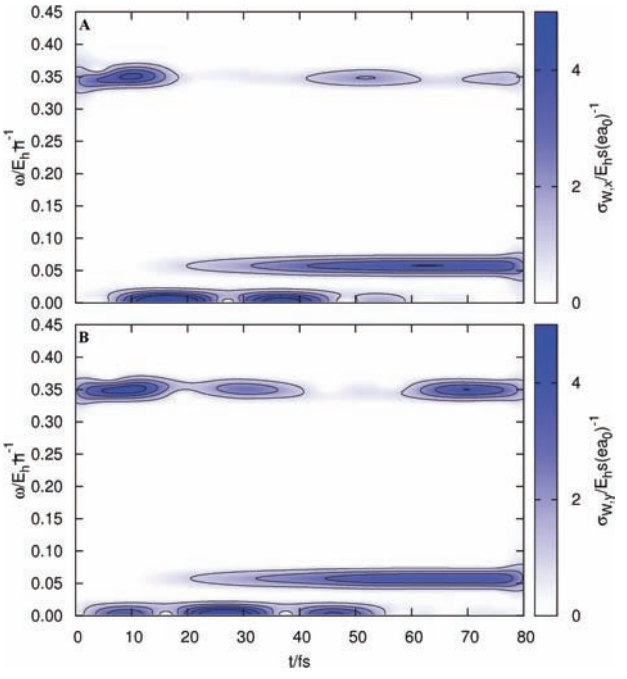

Figure 3. Time-dependent spectrum of the electric field for switching to target state (ii), using a Gaussian sliding window. **A** *x*-component; **B** *y*-component of the electric field vector.

and all population is shifted to states S_3/S_4. At $t \approx 10$ fs, states S_5/S_6 are populated. Starting at $t \approx 30$ fs, the population of state S_1 is slowly rising up to 45% at the end of the propagation. The final state contains 55% of state S_0 and 45% of state S_1.

State (ii) also has to be prepared taking a nondirect route. The transition dipole moments and energy differences are shown in Table 2. The trial pulse to start the OCT calculation is polarized in *y*-direction and 200 fs long. The sequence followed is

$$S_0 \rightarrow S_0 + S_4 \rightarrow S_0 + S_5 \rightarrow S_0 + S_2$$

In the first step, 50% of the population is transferred to state S_4, and in the subsequent steps all population from S_4 is transferred to state S_2 via S_5. In the laser pulse optimization, the electric field

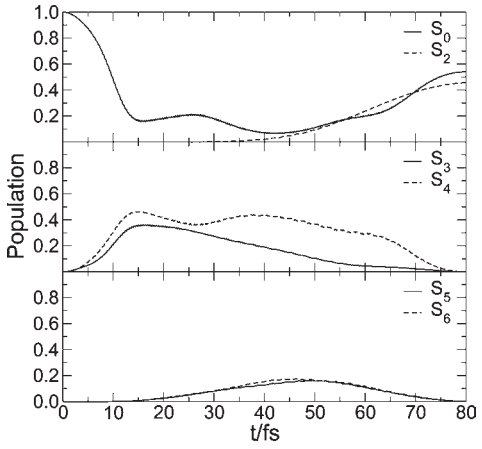

Figure 4. Populations of the electronic states involved in the population transfer from the ground state S_0 to the superposition of S_0 and S_2 (state (ii)).

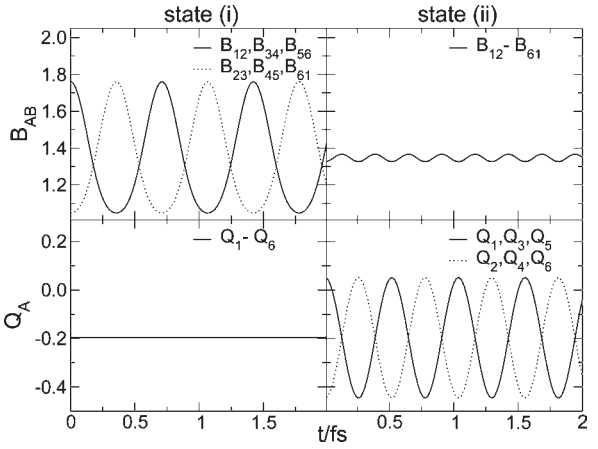

Figure 5. Time-dependent bond orders B_{AB} (top) and Mulliken charges Q_A (bottom) of the final states (i) (left) and (ii) (right).

vector is allowed to change in *x*- and *y*-polarization direction, so that the final pulse is an elliptically polarized pulse.[49,50] Using a step function, the pulse is shortened subsequently to 80 fs (see above). For shorter laser pulses, the final state could not be achieved as the desired superposition, where we allowed a deviation of 5% from a 1:1 superposition. The parameter for the optimized electric field is $\alpha_0 = 10\ (ea_0)^2 E_h^{-1}$. The frequency composition of the laser pulse at different times *t* is shown in Figure 3. At first, frequency components for the transition $S_0 \rightarrow S_3/S_4$ ($\omega \approx 0.35\ E_h\hbar^{-1}$) are contained in the laser pulse for both polarization directions. About 5−10 fs after the beginning of the pulse, the frequency components for the transitions $S_3/S_4 \rightarrow S_5/S_6$ ($\omega \approx 0.003\ E_h\hbar^{-1}$) are obtained, and at $t = 35$ fs, the population is transferred from S_5/S_6 to state S_2 (frequency components of $0.055\ E_h\hbar^{-1}$).

The populations of the states involved in the population transfer during the optimized laser pulse are shown in Figure 4. Almost 80% of the population is transferred from S_0 to S_3/S_4 at the beginning of the pulse. At $t \approx 20$ fs, states S_5 and S_6 are populated. From here, the population is shifted to state S_2 at around 40 fs. The final state contains 55% S_0 and 45% S_2.

In OCT calculations, care has to be taken to avoid too intense electric fields. Here, the maximum intensity of the optimized pulse (i) is $I_{max} = c\varepsilon_0|\varepsilon_{opt,max}|^2 = 7.05\ TW\ cm^{-2}$; (ii) $I_{max} = 0.79\ TW\ cm^{-2}$ (with *c* the speed of light, ε_0 the dielectric constant, and $\varepsilon_{opt,max}$ the maximum field amplitude). Competing processes such as bond breaking or ionization occur above a certain threshold I_{thr} which is typically between 1 and 10 $TW\ cm^{-2}$ for molecules. Thus, for target state (i), competing processes cannot be completely ruled out, but for target state (ii), the maximum intensity of the laser pulse is well below the threshold value. Furthermore, the ionization potential of benzene is IP = $0.3291\ E_h$ according to Koopmans' theorem, which is large compared to the energy uptake of the molecule during the laser pulse ($0.1069\ E_h$ in case of target state (i); $0.1466\ E_h$ for target state (ii)). The shapes of the optimized laser pulses ε_{opt} are shown in the Supporting Information.

Evolution of the Target States. After a complete switching of the electronic ground state to the selected target states (i) and (ii) is achieved, the target states can be propagated in time to calculate time-dependent properties. In particular, we are interested in the time-dependent Mulliken charges and bond orders, since these should indicate nonaromatic states (see above).

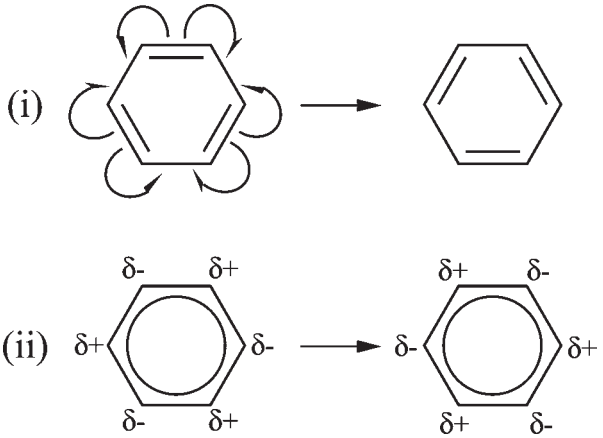

Figure 6. Lewis structures corresponding to states (i) (top) and (ii) (bottom).

The bond orders and Mulliken charges for the target states are shown in Figure 5. For state (i) (left part of the Figure), the bond orders oscillate in time, while the Mulliken charges remain constant. The opposite behavior is obtained for state (ii) (right part of Figure 5): Here, the bond orders remain almost constant, while the Mulliken charges oscillate. Taking a closer look at target state (i), we observe that the bond orders of the bonds between carbon atoms 1−2, 3−4, and 5−6 have an equal value at same times, as have the bonds between atoms 2−3, 4−5, and 6−1. When the bond orders of the former are at their maximum (value of 1.75), the bond orders of the latter are at their minimum (bond order of 1.05), resembling the Kekulé structure (see Figure 6). When this state is propagated in time (without applying an electric field), the bond orders oscillate between 1.75 and 1.05, while the Mulliken charges remain almost constant. Thus, each of the double bonds is split between two atoms, and one of the electrons is shifted clockwise to the next CC bond, and one counterclockwise, such that a single bond remains. If both electrons were shifted either clockwise or counterclockwise, the Mulliken charge of one atom would increase and the charge of the other former double-bonded atom would decrease. Also, such an electron shifting is dictated by symmetry: Target state (i) is of $^1A_{1g}$ symmetry, therefore the electron flow must obey symmetry with respect to the mirror planes $3\sigma_d$.

For target state (ii), the bond orders remain almost constant at a value of 1.30−1.35, slightly below the value of the aromatic ground state. The Mulliken charges of atoms C1, C3, and C5 are equal, as are the ones of atoms C2, C4, and C6, and the charges oscillate by a magnitude of 0.5 between a value of −0.45 and 0.05. When one set of atoms has a negative partial charge, the other set has a slightly positive partial charge. This state is a more or less triply ionic state, where part of the former six conjugated electrons is localized on three carbon atoms, and the remaining part is still delocalized over the ring system (see Figure 6). The partial charges are shifted from one carbon atom to another with time, resulting in two overlaying ring currents: one clockwise and one counterclockwise ring current. In the same manner as for target state (i), state (ii) has to obey the correct symmetric behavior of the wave function (symmetry with respect to the mirror planes $3\sigma_v$).

An unidirectional ring current can only be supported for superposition states of the same energy, that is, degenerate states.[51] Such ring currents have, for example, been predicted by Kanno et al., where also a switching of the current directions has been achieved.[52,53]

To estimate the number of electrons that are moving, we use the bond order and Mulliken charge differences: if a bond order of 1.0 corresponds to a single bond, where two electrons are involved in the bonding, then a bond order difference of 0.7 for state (i) corresponds to 1.4 electrons per shifted bond. Since there are three bonds which are shifted around, a total of 4.2 electrons is moving around the ring system. In the case of state (ii), the Mulliken charge differences between the partial positive and partial negative charges corresponds directly to the number of electrons moving, which is 1.5 electrons in total. However, this is a semiquantitative estimate; for a reliably estimation of the amount of charge moving see, for example, ref 54. Nevertheless, we do not aim at a further quantitative analysis of the electron flow, but rather use bond orders and Mulliken charges to analyze the target states.

One circulation around the ring system takes about 2.15 fs for state (i) (1.56 fs, state (ii)), so that shifting the electrons from one bond to the other (one carbon atom to the other, state (ii) takes 0.36 fs (0.26 fs, state (ii)). The oscillation period of the electronic motion (the time difference between two maxima in Figure 5) is 0.72 fs for state (i) (0.52 fs, state (ii)) and can be related to the energy differences between the states involved in the superposition: The energy difference between states S_0 and S_1 is 0.2932 E_h, which corresponds to 0.72 fs (state i), and the energy difference between states S_0 and S_2 is 0.2932 E_h, corresponding to 0.52 fs (state (ii)).

We have shown that by controlling the electron dynamics we can selectively switch benzene into nonaromatic target states. These target states exhibit an ultrafast bidirectional electron circulation around the ring system. In these states, the chemical properties of benzene will have significantly changed, e.g. leading to an enhanced reactivity and different ^{1}H NMR shieldings. Furthermore, electronic motion on the attosecond time scale can be measured using pump−probe photoelectron spectroscopy.[55,56]

We have also shown that the bonding in nonaromatic state (i) is not static; same as the partial positive and negative charges in structure (ii) cannot be attributed to certain carbon atoms. In both forms, the electrons show a dynamic behavior and we need more than a single Lewis structure to depict the bonding. Such a dynamic behavior has already been predicted by Shaik.[57] Using new ultrafast experimental techniques, this dynamic bonding can be probed.[55−57]

■ ASSOCIATED CONTENT

Supporting Information. Pulse shapes and parameters of the initial and final laser pulse and the atomic coordinates of the optimized geometry of benzene, together with the absolute RHF and CISD(18,18) energies. This material is available free of charge via the Internet at http://pubs.acs.org.

■ AUTHOR INFORMATION

Corresponding Author
inga.ulusoy@mytum.de

■ ACKNOWLEDGMENT

This work was supported by the Munich Centre for Advanced Photonics.

■ REFERENCES

(1) Feringa, B. L. *Molecular Switches*; Wiley-VCH: Weinheim, Germany, 2001.
(2) Barth, I.; Manz, J.; Shigeta, Y.; Yagi, K. *J. Am. Chem. Soc.* **2006**, *128*, 7043.
(3) Barth, I.; Manz, J. *Angew. Chem., Int. Ed.* **2006**, *45*, 2962.
(4) Korolkov, M. V.; Manz, J.; Paramonov, G. K. *Chem. Phys.* **1997**, *217*, 341.
(5) Chelkowski, S.; Bandrauk, A. D. *J. Chem. Phys.* **1993**, *99*, 4279.
(6) Remacle, F.; Nest, M.; Levine, R. D. *Phys. Rev. Lett.* **2007**, *99*, 183902.
(7) Nest, M.; Remacle, F.; Levine, R. D. *New J. Phys.* **2008**, *10*, 025019.
(8) Shaik, S.; Shurki, A.; Danovich, D.; Hiberty, P. C. A *Chem. Rev.* **2001**, *101*, 1501.
(9) Jug, K.; Hiberty, P. C.; Shaik, S. *Chem. Rev.* **2001**, *101*, 1477.
(10) Bach, R. D.; Wolber, G. J.; Schlegel, H. B. *J. Am. Chem. Soc.* **1985**, *107*, 2837.
(11) Jug, K.; Köster, A. M. *J. Am. Chem. Soc.* **1990**, *112*, 6772.
(12) Pierrefixe, S. C. A. H.; Bickelhaupt, F. M. *Chem.—Eur. J.* **2007**, *13*, 6321.
(13) Baird, N. C. *J. Am. Chem. Soc.* **1972**, *94*, 4941.
(14) Malar, E. J. P.; Jug, K. *J. Phys. Chem.* **1984**, *88*, 3508.
(15) Karadakov, P. B. *J. Phys. Chem. A* **2008**, *112*, 7303.
(16) Stepień, M.; Latos-Grażyński, L; Sprutta, N.; Chwalisz, P; Szterenberg, L *Angew. Chem.* **2007**, *119*, 8015.
(17) Reinhard, P.-G.; Suraud, E. In *Time-Dependent Density Functional Theory*; Marques, M., Ullrich, C., Nogueira, F., Rubio, A., Burke, K., Gross, E., Eds.; Lecture Notes in Physics; Springer: Berlin, 2006; Vol. 706; pp 391−406.
(18) Messud, J.; Dinh, P. M.; Reinhard, P.-G.; Suraud, E. *Phys. Rev. Lett.* **2008**, *101*, 096404.
(19) Karna, S. P.; Dupuis, M. *J. Comput. Chem.* **1991**, *12*, 487.
(20) Kato, T.; Kono, H. *Chem. Phys. Lett.* **2004**, *392*, 533.
(21) Nest, M.; Klamroth, T.; Saalfrank, P. *J. Chem. Phys.* **2005**, *122*, 124102.
(22) Klamroth, T.; Nest, M. *Phys. Chem. Chem. Phys.* **2009**, *11*, 349.
(23) Kato, T.; Kono, H. *J. Chem. Phys.* **2008**, *128*, 184102.
(24) Padmanaban, R.; Nest, M. *Chem. Phys. Lett.* **2008**, *463*, 263.
(25) Kuleff, A. I.; Breidbach, J.; Cederbaum, L. S. *J. Chem. Phys.* **2005**, *123*, 044111.
(26) Cederbaum, L. S. *J. Chem. Phys.* **2008**, *128*, 124101.
(27) Krause, P.; Klamroth, T.; Saalfrank, P. *J. Chem. Phys.* **2005**, *123*, 074105.
(28) Zhu, W.; Rabitz, H. *J. Chem. Phys.* **1998**, *109*, 385.
(29) Schleyer, P. v. R.; Maerker, C.; Dransfeld, A.; Jiao, H.; Hommes, N. J. R. v. E. *J. Am. Chem. Soc.* **1996**, *118*, 6317.
(30) Chen, Z.; Wannere, C. S.; Corminboeuf, C.; Puchta, R.; Schleyer, P. v. R. *Chem. Rev.* **2005**, *105*, 3842.

(31) Taubert, S.; Sundholm, D.; Jusélius, J. *J. Chem. Phys.* **2011**, *134*, 054123.
(32) Pelloni, S.; Lazzaretti, P. *J. Phys. Chem. A* **2011**, *115*, 4553.
(33) Kertesz, M.; Choi, C. H.; Yang, S. *Chem. Rev.* **2005**, *105*, 3448.
(34) Boldyrev, A. I. *Chem. Rev.* **2005**, *105*, 3716.
(35) Mayer, I. *Int. J. Quantum Chem.* **1986**, *29*, 73.
(36) Mulliken, R. S. *J. Chem. Phys.* **1955**, *23*, 1833.
(37) Matito, E.; Solá, M.; Salvador, P.; Duran, M. *Faraday Discuss* **2007**, *135*, 325.
(38) Matito, E.; Poater, J.; Solá, M.; Duran, M.; Salvador, P. *J. Phys. Chem. A* **2005**, *109*, 9904.
(39) Jug, K. *J. Org. Chem.* **1983**, *48*, 1344.
(40) Bandrauk, A. D.; Aubanel, E.; Chelkowski, S. In *Femtosecond Chemistry*; Manz, J., Wöste, L., Eds.; Verlag Chemie: New York, 1995; Vol. 2; Chapter 25, p 731.
(41) Bandrauk, A. D.; Shen, H. *J. Chem. Phys.* **1993**, *99*, 1185.
(42) Hehre, W. J.; Stewart, R. F.; Pople, J. A. *J. Chem. Phys.* **1969**, *51*, 2657.
(43) Hehre, W. J.; Ditchfield, R.; Stewart, R. F.; Pople, J. A. *J. Chem. Phys.* **1970**, *52*, 2769.
(44) Bochicchio, R. C.; Lain, L.; Torre, O. *Chem. Phys. Lett.* **2003**, *374*, 567.
(45) Mayer, I. *J. Comput. Chem.* **2006**, *28*, 204.
(46) Bally, T.; Masamune, S. *Tetrahedron* **1980**, *36*, 343.
(47) Shaik, S.; Shurki, A.; Danovich, D.; Hiberty, P. C. *J. Am. Chem. Soc.* **1996**, *118*, 666.
(48) Shaik, S. S.; Hiberty, P. C. *A Chemist's Guide to Valence Bond Theory*; Wiley-Interscience: 2008; Chapter 7, p 200.
(49) Yuan, K.-J.; Bandrauk, A. D. *Phys. Rev. A* **2011**, *83*, 063422.
(50) Yuan, K.-J.; Bandrauk, A. D. *Phys. Rev. A* **2010**, *81*, 063402.
(51) Barth, I. Quantum control of electron and nuclear circulations, ring currents, and induced magnetic fields in atoms, ions and molecules by circularly polarized laser pulses. Ph.D. thesis, Freie Universität Berlin.
(52) Kanno, M.; Hoki, K.; Kono, H.; Fujimura, Y. *J. Chem. Phys.* **2007**, *127*, 204314.
(53) Kanno, M.; Kono, H.; Fujimura, Y. *Angew. Chem., Int. Ed.* **2006**, *45*, 7995.
(54) Hege, H.-C.; Manz, J.; Marquardt, F.; Paulus, B.; Schild, A. *Chem. Phys.* **2010**, *376*, 46.
(55) Bandrauk, A. D.; Chelkowski, S.; Corkum, P. B.; Manz, J.; Yudin, G. L. *J. Phys. B: At. Mol. Opt. Phys.* **2009**, *42*, 134001.
(56) Bandrauk, A. D.; Chelkowski, S.; Nguyen, H. S. *Int. J. Quantum Chem.* **2004**, *100*, 834.
(57) Shaik, S. *J. Comput. Chem.* **2007**, *28*, 51.